CO_2 Capture by Absorption with Potassium Carbonate

Quarterly Progress Report
Reporting Period Start Date: October 1, 2004
Reporting Period End Date: December 31, 2004
Authors: Gary T. Rochelle, J. Tim Cullinane, Marcus Hilliard,
Eric Chen, Babatunde Oyenekan, and Ross Dugas

January 31, 2005
DOE Award #: DE-FC26-02NT41440
Department of Chemical Engineering
The University of Texas at Austin

Disclaimer

Abstract

The objective of this work is to improve the process for CO_2 capture by alkanolamine absorption/stripping by developing an alternative solvent, aqueous K_2CO_3 promoted by piperazine. Thermodynamic modeling predicts that the heat of desorption of CO_2 from 5m K+/2.5 PZ from 85 kJ/mole at 40^{o}C to 30 kJ/mole at 120^{o}C. Mass transfer modeling of this solvent suggests that carbonate and general salt concentration play a major role in catalyzing the rate of reaction of CO_2 with piperazine. Stripper modeling suggests that with the multipressure stripper, the energy consumption with a generic solvent decreases by 15% as the heat of desorption is decreased from 23.8 to 18.5 kcal/gmol. A second pilot plant campaign with 5m K+/2.5 PZ was successfully completed.

Contents

Disclaimer 2
Abstract 3
List of Figures 5
List of Tables 6
Introduction 7
Experimental 7
Results and Discussion 7
Conclusions 8
Future Work 8

Task 1 – Modeling Performance of Absorption/Stripping of CO_2 with Aqueous K_2CO_3 Promoted by Piperazine 10
Subtask 1.1b – Modify Vapor-Liquid Equilibrium (VLE) Model – Aspen Plus® 10
Subtask 1.2 – Modify Point Rate Model 14
Introduction 14
Methods 14
Results 15
Conclusions 19

Subtask 1.3a – Develop Integrated Absorber/Stripper Model – Aspen Custom Modeler® for Stripper 20
Introduction 20
Experimental (Model Formulation) 20
Results and Discussion 22
Conclusions and Future Work 23

Task 2 – Pilot Plant Testing 25
Subtask 2.5a – Campaign 2 Pilot Plant – Results for Absorber 25
Introduction 25
Experimental 25
Results and Discussion 26
Conclusions and Future Work 30
Subtask 2.5b – Campaign 2 Pilot Plant – Results for Stripper 31
Summary 31
Experimental 31
Results and Discussion 31
Conclusions and Future Work 37
Subtask 2.7a – MEA Baseline Campaign – Development of Online Conductivity Measurements 38
Introduction 38
Experimental 38
Results and Discussion 38
References 42

Figures

Figure 1 Comparison of Electrolyte-NRTL Predictions with UNIFAC-DMD Predictions for the Activity Coefficient of PZ from 298 to 323 K

Figure 2 Predictions for the Heat of CO_2 Absorption from the Electrolyte-NRTL Model in a 1.8 m PZ Solution from 313 to 393 K

Figure 3 Predictions for the Heat of CO_2 Absorption from the Electrolyte-NRTL Model in a 5 m K^+/2.5 m PZ Solution from 313 to 393 K

Figure 4 Effect of Ionic Strength on the Apparent Rate Constant and Physical Parameters in 0.6 m PZ [Closed Points: 25°C Experiments, Open Points: 60°C Experiments, Lines: Model for K_2CO_3/PZ ($k_{2,app}$ excludes CO_3^{2-} catalysis effect)]

Figure 5 Normalized Flux in K^+/PZ Mixtures at 60°C [Points: Experimental Data (MEA from Dang [2001]), Lines: Model Prediction ($k_l^o = 1\times10^{-4}$ m/s, $P_{CO2,i} = 3.0\times P_{CO2}^*$)]

Figure 6 Temperature Dependence of Normalized Flux of 5.0 m K^+/2.5 m PZ [Points: Experimental Data, Lines: Model Prediction ($k_l^o = 1\times10^{-4}$ m/s, $P_{CO2,i} = 3.0\times P_{CO2}^*$)]

Figure 7 Approximate Solutions to Normalized Flux in 5.0 m K^+/2.5 m PZ at 60°C, $k_l^o = 1.0\times10^{-4}$ m/s, $P_{CO2,i} = 1.05\times P_{CO2}^*$

Figure 8 Performance Curves for Generic Solvents

Figure 9 Wetted Wall Column and Campaign 1 Rate Data

Figure 10 Pinched Data Points from Campaign 1

Figure 11 Temperature Profiles in the Stripper at Different Pressures to Yield 85% Removal

Figure 12 Ionic Conductivity Sensitivity to Loading at 15 Wt% MEA

Figure 13 Ionic Conductivity Sensitivity to MEA Wt% at ~0.20 Loading

Tables

Table 1 Absolute Percent Relative Error for the H_2O-K_2CO_3-CO_2 Model

Table 2 Absolute Average Percent Relative Error for the H_2O-K_2CO_3-PZ-CO_2 Optimum Model

Table 3 Average Percent Absolute Error for the H_2O-K_2CO_3-PZ-CO_2 Optimum Model

Table 4 Adjustable Constants in VLE Expression

Table 5 Rich $[CO_2]_T$ at Absorber Conditions at 60^oC

Table 6 Stripper Performance for Three Generic Solvents

Table 7 Performance of Generic Solvents with Multipressure Stripper, Rich P_{CO2}*= 5kPa

Table 8 Absorber Results Table

Table 9 Campaign 2 Stripper Data

Table 10 Energy Efficiency of Stripping Operations

Table 11 Liquid Phase Analysis for Stripper

Table 12 Ionic Conductivity, Temperature, and Loading Raw Data

Table 13 Regressed Parameters and Error Analysis

Introduction

The objective of this work is to improve the process for CO_2 capture by alkanolamine absorption/stripping by developing an alternative solvent, aqueous K_2CO_3 promoted by piperazine. This work expands on parallel bench scale work with system modeling and pilot plant measurements to demonstrate and quantify the solvent process concepts.

The bench-scale and modeling work is supervised by Gary Rochelle. Frank Seibert is supervising the pilot plant. Three graduate students (Ross Dugas, Jennifer Lu, and Babatunde Oyenekan) have received support during this quarter for direct effort on the scope of this contract. Four students supported by other funding have made contributions this quarter to the scope of this project (Eric Chen – EPA Star Fellowship; Tim Cullinane and Marcus Hilliard – Industrial Research Associates, Babatunde Oyenekan – teaching assistantship and Trimeric).

Experimental

Subtask 2.5 describes the methods used in the pilot plant for the second campaign.

Subtask 2.7 includes experimental methods for measuring the physical properties of MEA solutions.

Results and Discussion

Progress has been made on three subtasks in this quarter:

Subtask 1.1 – Modify Vapor-Liquid Equilibrium (VLE) Model

Marcus Hilliard has completed a Non-Random Two-Liquid (NRTL) Electrolyte model in AspenPlus to represent all of the available thermodynamic data on the system potassium carbonate-piperazine-water-carbon dioxide.

Subtask 1.2 – Modify Point Rate Model

Tim Cullinane has developed rate parameters in the rigorous Bishnoi model to represent the rates of CO_2 absorption and desorption measured in the wetted wall column at both absorber and stripper conditions.

Subtask 1.3 – Develop Integrated Absorber/Stripper Model

Babatunde Oyenekan has used the stripper model to calculate the effect of the heat of desorption with a generic solvent like MEA.

Subtask 2.5 – Pilot Plant – Campaign 2

Campaign 2 was completed in October 2004 with 23 runs and eight full days of pilot plant data.

Subtask 2.7 – Pilot Plant – Campaign 3 – MEA Baseline

Electrical conductivity and density was measured in loaded solutions of MEA to facilitate on-line measurement of CO_2 loading in Campaign 3.

Conclusions

1. The AspenPlus electrolyte-NRTL for H_2O-K_2CO_3-PZ- CO_2 systems represents the data for CO_2 solubility with an average error of 14% and the speciation data with an average error of 4%.
2. At typical lean loading, the predicted heat of CO_2 desorption varies from 85 kJ/mole at 40^oC to 30 kJ/mole at 120^oC.
3. Expanded experiments on aqueous PZ revealed that the kinetics approach second-order behavior with the amine.
4. The presence of high ionic strength has a significant impact on the absorption rate of CO_2. Studies of neutral salts show that kinetics are enhanced, but the physical solubility and diffusivity of CO_2 are reduced. The net effect is a diminished absorption rate.
5. Concentrated K^+/PZ mixtures demonstrate favorable absorption rate characteristics, outperforming current state-of-the-art technologies such as 5 M MEA. At low temperatures, kinetics control the absorption rate. At high temperatures, the rate may be limited by physical CO_2 solubility.
6. A series addition approximation of PFO and instantaneous behavior adequately represents the absorption rate at low driving forces. At moderate to high loadings, the absorption rate approaches an instantaneous condition.
7. With the multipressure stripper, the energy consumption with a generic solvent decreases by 15% as the heat of desorption is decreased form 23.8 to 18.5 kcal/gmol.
8. Foaming was encountered in campaign 2 in the plant plant. It was resolved with an antifoaming additive.
9. The CO_2 material balance in Campaigns 1 and 2 has been resolved within the precision of the measurements (10%).
10. The temperature profiles in the stripper suggest that it was limited by a lean end pinch at 0.3 and 1.6 atm and by a rich end pinch at 3.4 atm.

Future Work

We expect the following accomplishments in the next quarter:

Subtask 1.1 – Modify Vapor-Liquid Equilibrium (VLE) Model

The M.S. thesis by Marcus Hilliard will be submitted as a separate topical report on this completed work.

Subtask 1.2 – Modify Point Rate Model

The Ph.D. dissertation by Tim Cullinane will be submitted as a separate topical report on this completed work.

Subtask 1.3 – Develop Integrated Absorber/Stripper Model

In the next quarter, a mass transfer rate model will be developed to predict the height of packing required to perform the stripping of CO_2 using various solvents with minimum energy consumption.

The existing absorber model for MEA will be modified to accept piperazine species.

Subtask 1.5 – Simulate Base Case Pilot

The absorber data from Campaigns 1 and 2 will be simulated with a rigorous differential equation model.

The stripper data from Campaigns 1 and 2 will be analyzed with the model developed in Aspen Custom Modeler®.

Subtask 2.1 – Pilot Plant Test Plan

A detailed test plan will be developed for the third pilot plant campaign, the MEA base case.

Subtask 2.7 – MEA Baseline

The third pilot plant campaign, the MEA base case, is scheduled to be completed in the next quarter.

Task 1 – Modeling Performance of Absorption/Stripping of CO_2 with Aqueous K_2CO_3 Promoted by Piperazine

Subtask 1.1b – Modify Vapor-Liquid Equilibrium (VLE) Model – Aspen Plus®

by Marcus Hilliard
(Supported by the Industrial Associates Program for CO_2 Capture by Aqueous Absorption)

The Electrolyte NRTL Activity Coefficient model within Aspen Plus® v12.1 was used to develop a rigorous thermodynamic representation of an aqueous piperazine (PZ) and potassium carbonate (K_2CO_3) mixed-solvent electrolyte system for the application of carbon dioxide (CO_2) absorption/stripping from power plant flue gas. The model predicts the speciation and carbon dioxide solubility as a function of solvent composition, temperature, and pressure. These results provide the capacity of the solvent, the heat of absorption, and the concentration of reactive species (e.g., piperazine and piperazine carbamate ($PZCOO^-$)).

This work is completely reported in a master's thesis (Hilliard, 2005). This thesis will be submitted to DOE as a separate topical report. A summary of this work follows below.

Binary interaction parameters for the potassium carbonate/piperazine mixed-solvent electrolyte system were obtained through the regression of water vapor pressure and calorimetry over potassium carbonate and potassium bicarbonate ($KHCO_3$) solutions, CO_2 solubility in potassium carbonate/piperazine, and proton nuclear magnetic resonance (NMR) of potassium carbonate/piperazine speciation.

Speciation data for determining binary interaction parameters is included as a key feature of this work since it enhances the predictive capabilities of Aspen Plus® to accurately predict liquid phase compositions.

As a result, the model adequately describes mean ionic activity coefficient data in aqueous K_2CO_3 mixtures within average absolute relative error (AARD) of ± 8.5%, CO_2 solubility data in aqueous K_2CO_3- CO_2 mixtures within AARD of +/- 11%, and exhibits a weak effect of K+ presented in the CO_2 solubility data and heat capacity predictions as shown in Table 1.

Table 1. Absolute Percent Relative Error for the H_2O-K_2CO_3-CO_2 Model

	%AARD	Max.
H_2O/K_2CO_3 System		
Vapor Pressure Depression - Aseyev (1999) & Puchkov and Kurochkina (1970)	1.0	7.7
Heat Capacity of Solution - Aseyev and Zaytsev (1996)	1.1	4.0
Mean Ionic Activity Coefficient - Aseyev and Zaytsev (1996)	8.5	24.7
$H_2O/KHCO_3$ System		
Vapor Pressure Depression - Aseyev (1999)	0.4	0.6
Heat Capacity of Solution - Aseyev and Zaytsev (1996)	1.0	3.4
$H_2O/K_2CO_3/CO_2$ System		
CO_2 Solubility (P^*_{CO2}) - Tosh *et al.* (1959)		
20 wt% K_2CO_3	10	33
30 wt%	12	39
40 wt%	11	45
Overall	2.3	45

Predicting the activity coefficient behavior of aqueous PZ from a purely predictive property may or may not capture experimental trends; the model exhibits systematic errors presented in the infinite dilution activity coefficient for PZ as temperature increases even though all the predictions of the model were within an AARD of +/- 1.2%, with the exception of a few outliers as shown in Figure 1.

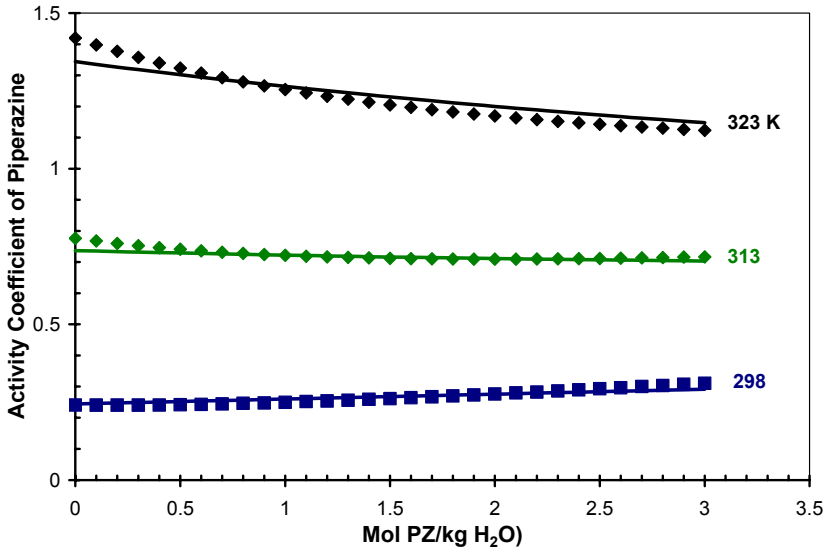

Figure 1. Comparison of Electrolyte-NRTL Predictions with UNIFAC-DMD Predictions for the Activity Coefficient of PZ from 298 to 323 K

Gathering experimental data for the activity coefficient of aqueous PZ and other thermodynamic and calorimetric data for solutions at various loadings will help to validate model predictions from various authors.

In addition, the model adequately describes total pressure and CO_2 solubility data within an AARD of +/- 14.2% and proton NMR speciation within an average absolute error (ARD) of +/- 2.3%, with the exception of a few outliers for the H_2O-PZ- CO_2 and H_2O-K_2CO_3-PZ- CO_2 systems.

Table 2. Absolute Average Percent Relative Error for the H_2O-K_2CO_3-PZ-CO_2 Optimum Model

H_2O/PZ/CO_2 System

	AARD (%)	Max.
Total Pressure - Pérez-Salado Kamps *et al* . (2003)	15.9	35.2
CO_2 Solubility - Bishnoi (2000)	11.8	47.8
H_2O/K_2CO_3/PZ/CO_2 System		
CO_2 Solubility - Cullinane and Rochelle (2005)	13.8	28.2

Table 3. Average Percent Absolute Error for the H_2O-K_2CO_3-PZ-CO_2 Optimum Model

H_2O/PZ/CO_2 System

	AAD (%)		
	PZ/PZH^+	$PZCOO^-/H^+PZCOO^-$	$PZ(COO^-)_2$
Proton NMR Speciation - Ermatchkov *et al* . (2003)	1.8	2.2	1.2
H_2O/K_2CO_3/PZ/CO_2 System			
	PZ/PZH^+	$PZCOO^-/H^+PZCOO^-$	$PZ(COO^-)_2$
Proton NMR Speciation - Cullinane and Rochelle (2005)	3.0	3.9	4.3

Using the model for its predictive capabilities, the heat of CO_2 absorption for 1.8 m PZ mixtures from 313 to 393 K was found to demonstrate strong non-linear temperature dependence as a function of loading as shown in Figure 2.

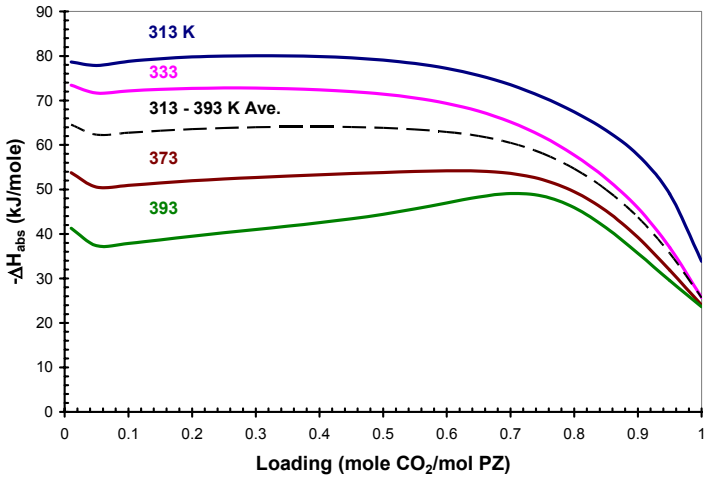

Figure 2. Predictions for the Heat of CO_2 Absorption from the Electrolyte-NRTL Model in a 1.8 m PZ Solution from 313 to 393 K

Also, the heat of CO_2 absorption for 5 m K^+/2.5 m PZ mixtures from 313 to 393 K was found to also demonstrate a strong non-linear temperature dependence as a function of loading < 0.7. At loadings above ~0.72, the non-linear temperature dependence for the heat of CO_2 absorption collapses to approximately a linear function with respect to loading approaching the heat of CO_2 absorption corresponding to the physical absorption of CO_2 as shown in Figure 3. Since the heat of CO_2 absorption is a purely predictive property, gathering experimental data for the heat of CO_2 absorption and the heat capacity for solutions at various loadings will help to validate model predictions from various authors.

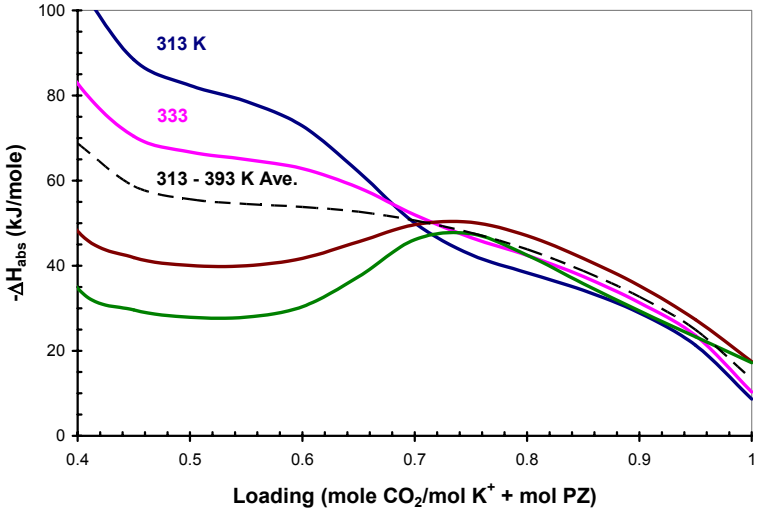

Figure 3. Predictions for the Heat of CO_2 Absorption from the Electrolyte-NRTL Model in a 5 m K^+/2.5 m PZ Solution from 313 to 393 K

In conclusion, the model satisfactorily correlates the experimental data of this mixed-solvent electrolyte system over a wide range of temperatures, mixed-solvent concentration, and CO_2 loading.

Subtask 1.2 – Modify Point Rate Model

by J. Tim Cullinane
(Supported by the Industrial Associates Program for CO_2 Capture by Aqueous Absorption)

Introduction

Work has been completed on the point rate model for CO_2 absorption/desorption into potassium carbonate/piperazine. A journal manuscript has been prepared. The work will be more completely archived in a Ph.D. dissertation to be submitted as a DOE topical report in the next quarter. The text that follows is a summary of this work.

The removal of carbon dioxide from gas streams is important in both natural gas treating and in ammonia production with the potential for application to capture from combustion flue gas. Most large-scale gas treating processes include the absorption of the gases into a circulated chemical solvent in an absorber/stripper system. Aqueous amines and potassium carbonate (K_2CO_3) have been recognized as viable solvents for gas treating. These solvents are generally effective in removing CO_2, though performance is limited by the absorption rate. An understanding of the fundamental mechanisms dictating the rate is critical to developing more efficient capture processes.

Previous work has identified piperazine (PZ) as an effective promoter of CO_2 absorption rates in methyldiethanolamine (MDEA) and K_2CO_3 [Bishnoi and Rochelle (2002),]. This work presents the development of concentrated K^+/PZ for CO_2 capture.

Methods

The absorption rate of CO_2 into 0.0 to 6.2 m K^+ and 0.6 to 2.5 m PZ was measured in a wetted-wall column at 25 to 110°C. The wetted-wall column consists of a stainless steel tube with a total contact area of 38.52 cm^2. The contactor is insulated with a circulating heat transfer fluid.

The test solvent is circulated at 2 to 3 cm^3/s from a 1400 cm^3 reservoir. A N_2 and CO_2 mixture (0.01 to 10% CO_2) was saturated with water and sent to the column. After absorption/desorption into the solvent, the outlet CO_2 concentration was measured by infrared gas analyzers. Liquid samples were taken from the contactor during each experiment for inorganic carbon determination.

An expression of the liquid film resistance, including the kinetics of CO_2 absorption, was calculated from K_G, the overall mass transfer coefficient as determined by experiment, corrected by the gas film resistance, k_g.

$$k_g^{'} = \left(\frac{1}{K_G} - \frac{1}{k_g} \right)^{-1}$$

k_g' is a normalized flux, a mass transfer coefficient for the partial pressure driving force across the liquid film. If a pseudo-first order condition applies, k_g' can be written

$$k'_{g,PFO} = \frac{\sqrt{D_{CO_2} k_{app}}}{H_{CO_2}}$$

where D_{CO2} is the diffusion coefficient, H_{CO2} is the Henry's constant, and k_{app} is the apparent rate constant derived from the chosen kinetic representation.

A rigorous rate model, based on the model of Bishnoi (200), was constructed for describing the absorption of CO_2 through the gas-liquid boundary layer. The model was fit to experimental data by the regression of rate constants and diffusion coefficients.

Further details on the experimental apparatus, procedure, and model construction can be found in previous work [Cullinane and Rochelle (2004), Bishnoi (2000), Austgen (1989), and Posey (1996)].

Results

Aqueous PZ

Bishnoi (2000) measured the rate of CO_2 absorption into 0.2 and 0.6 M PZ at 25 to 60°C and zero loading and reported a rate constant assuming first-order rate dependence on PZ. The reported rate constant at 25°C is 53,700 m^3/kmol-s and the activation energy is 33,600 kJ/kmol. In this work, the absorption rate was measured in 0.45 to 1.5 m PZ at 25 and 60°C and zero loading. Data was also obtained in 0.6 m PZ containing 0.15 m KOH to quantify promotion effects of OH^-.

This work found a strong dependence of a second-order rate constant on PZ concentration, showing that the reaction is not first-order with PZ as had been previously assumed. As PZ concentration is increased above a concentration of 0.5 M, the reaction order approaches 2.

In addition to the second-order dependence on the amine, a significant rate enhancement is observed with hydroxide in solution. With 0.15 m KOH, the flux increases by a factor of two in 0.6 m PZ solution. This indicates that strong bases contribute to the overall reaction rate and must be included in the rate expression, consistent with a termolecular mechanism and base-catalysis theory [Bronsted (1928)].

Neutral Salt Effects

Given the high ionic strength present in concentrated K^+/PZ mixtures, a study was initiated on the effect of neutral salts on the absorption rate of CO_2 into aqueous amines. Figure 4 illustrates the influence of neutral salts in 0.6 m PZ on the apparent rate constant and important physical parameters, represented as $\sqrt{D_{CO_2}}/H_{CO_2}$. The addition of 1.8 M ionic strength increases the apparent rate constant by a factor of 2.5 at 25°C and 60°C. With 3 M KCl the apparent rate constant increases by a factor of 15. The rate model for K^+/PZ shows similar results.

It is important to recognize that ionic strength also changes the effective diffusion coefficient and physical solubility of CO_2; therefore, the interpretation of a rate constant strongly depends on the ability to estimate $\sqrt{D_{CO_2}}/H_{CO_2}$. In 3 M K_2CO_3, the parameter

decreases by 70%. The competing effects of kinetics and physical changes results in a diminishing value of absorption rate.

K^+/PZ Mixtures

The k_g' of several K^+/PZ solvents is shown in Figure 5. In promoted K_2CO_3 (i.e., 3.6 m K^+/0.6 m PZ), the absorption rate is fast, though 20 to 30% less than 5 M MEA. More concentrated solvents, such as 3.6 m K^+/1.8 m PZ, have absorption rates a factor of 1.5 higher than 5 M MEA.

Interestingly, 5.0 m K^+/2.5 m PZ has a normalized flux nearly identical to 3.6 m K^+/1.8 m PZ suggesting that more concentrated solvents do not necessarily yield faster absorption rates. This is somewhat unexpected since previous investigations of speciation suggest more reactive species are present at higher solvent concentrations [Cullinane and Rochelle (2005)]. The similarity in rates can be explained by the two mechanisms acting in neutral salts. The kinetics increase, but in more concentrated solvents, the viscosity is higher, leading to a smaller CO_2 diffusion coefficient and lower physical solubility. The competing effects of kinetics and diffusivity and solubility appear to play a significant role in determining the absorption rate in some solvents.

Figure 6 illustrates the dependence of normalized flux on temperature. At low to moderate temperatures (40 to 80°C), an increase in k_g' is observed with temperature. This corresponds to increasing kinetics and mass transfer properties that accompany a higher temperature. This is also observed at 100 to 110°C and low P_{CO2}*. At the high temperatures and high P_{CO2}*, a relatively small difference in k_g' is observed. This indicates an approach to instantaneous behavior, where the diffusion of reactants and products becomes limiting.

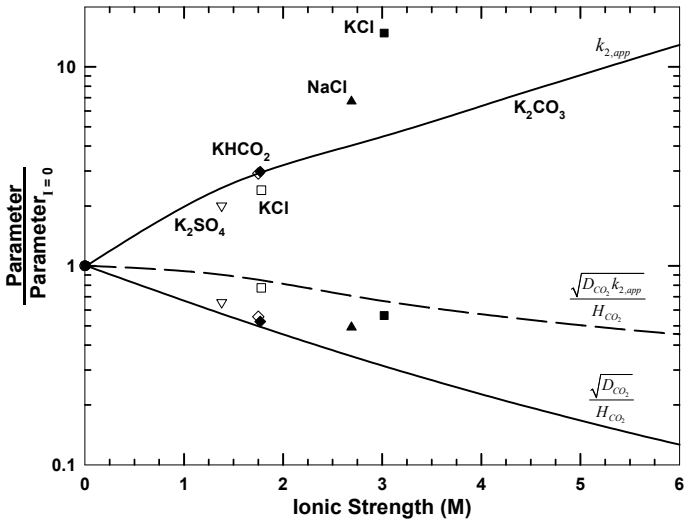

Figure 4. Effect of Ionic Strength on the Apparent Rate Constant and Physical Parameters in 0.6 m PZ [Closed Points: 25°C Experiments, Open Points: 60°C Experiments, Lines: Model for K_2CO_3/PZ ($k_{2,app}$ excludes CO_3^{2-} catalysis effect)]

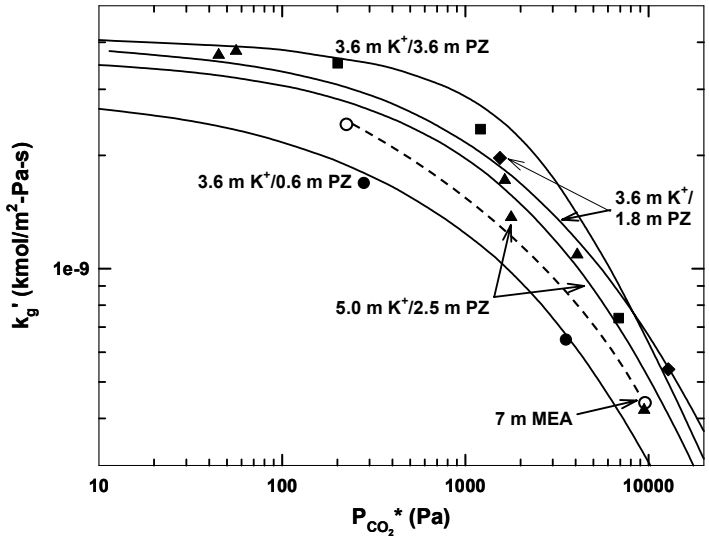

Figure 5. Normalized Flux in K^+/PZ Mixtures at 60°C [Points: Experimental Data (MEA from Dang [2001]), Lines: Model Prediction ($k_l^o = 1\times10^{-4}$ m/s, $P_{CO2,i} = 3.0\times P_{CO2}^*$)]

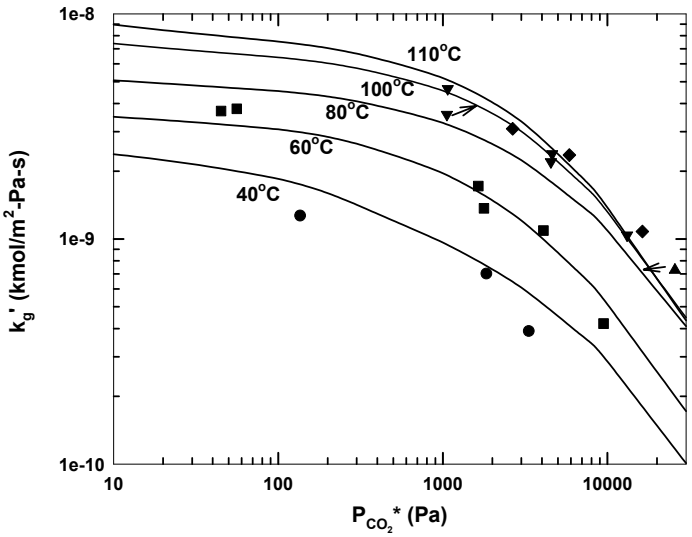

Figure 6. Temperature Dependence of Normalized Flux of 5.0 m K^+/2.5 m PZ [Points: Experimental Data, Lines: Model Prediction ($k_l^o = 1\times10^{-4}$ m/s, $P_{CO2,i} = 3.0\times P_{CO2}^*$)]

Approximate solutions to the rigorous model are sometimes appropriate in that simple calculations based on bulk properties are possible and more assessable than rigorous solutions. Additionally, simple models aid the understanding of complex physical phenomena. Solvent performance at typical experimental conditions was analyzed to determine the validity of the proposed approximations.

Figure 7 shows various representations of normalized flux at 60°C with a low driving force. At low loadings, k_g' is described well by pseudo-first order approximation, $k_g'_{,PFO}$, meaning that, if kinetics are known, a rigorous model of the boundary layer is not necessary. At high loadings, the reaction approaches an instantaneous condition and deviates from simple kinetic considerations.

Two representations of instantaneous reaction are possible: a global instantaneous condition, where all reactions are considered instantaneous and the absorption is limited by diffusion; and a PZ-instantaneous condition, where only PZ reactions are instantaneous. The values of $k_g'_{,PZ,INST}$ and $k_g'_{,GBL,INST}$ are approximately equal at low loadings, but diverge at high loadings, indicating an increase in the contribution of bicarbonate formation to the overall absorption rate relative to the reaction with PZ species.

It was found that a simple, series addition of the pseudo-first order approximation and the PZ-instantaneous condition provides a good representation of actual rate performance over the entire loading range at low driving forces.

$$k'_{g,SR} = \left(\frac{1}{k'_{g,PFO}} + \frac{1}{k'_{g,PZ,INST}} \right)$$

This means that at high loadings, though approaching an instantaneous and thus equilibrium controlled condition, kinetics are still important. Specifically, the formation of bicarbonate appears to be limiting.

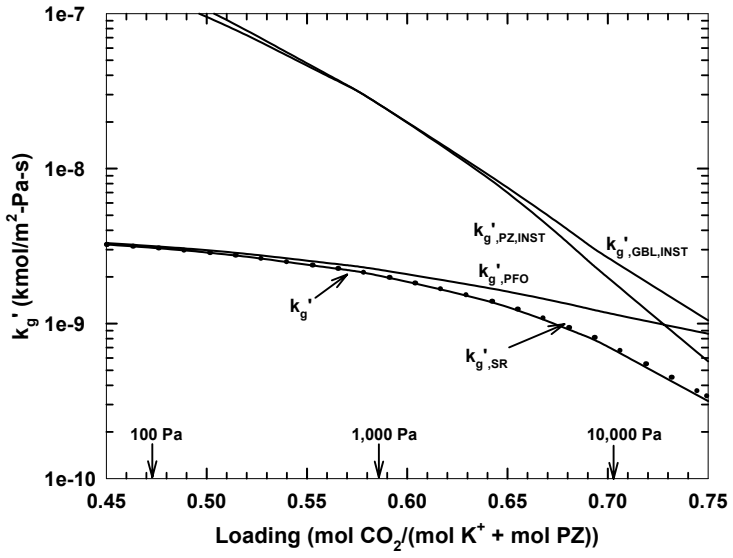

Figure 7. Approximate Solutions to Normalized Flux in 5.0 m K^+/2.5 m PZ at 60°C, $k_l^o = 1.0\times10^{-4}$ m/s, $P_{CO2,i} = 1.05\times P_{CO2}^*$

Conclusions

Expanded experiments on aqueous PZ revealed that the kinetics approach second-order behavior with the amine. The rate constants found agree with previous data at similar conditions.

The presence of high ionic strength has a significant impact on the absorption rate of CO_2. Studies of neutral salts show that kinetics are enhanced, but the physical solubility and diffusivity of CO_2 is reduced. The net effect is a diminished absorption rate.

Concentrated K^+/PZ mixtures demonstrate favorable absorption rate characteristics, outperforming current state-of-the-art technologies such as 5 M MEA. At low temperatures, kinetics control the absorption rate. At high temperatures, the rate may be limited by physical CO_2 solubility.

A series addition approximation of PFO and instantaneous behavior adequately represents the absorption rate at low driving forces. At moderate to high loadings, the absorption rate approaches an instantaneous condition.

Subtask 1.3a – Develop Integrated Absorber/Stripper Model – Aspen Custom Modeler® for Stripper

by Babatunde Oyenekan
(Supported by this contract)

Introduction

We have continued to develop the stripper submodel in Aspen Custom Modeler® for the overall model of CO_2 absorption/stripping by three generic solvents. This model divides the stripper into sections with Murphree efficiencies assigned to CO_2, water and temperature. A new expression with six adjustable constants is used to represent the VLE and heat of absorption/desorption. Two process configurations (a simple stripper and a multipressure stripper) are simulated and the effect of varying the rich and lean $[CO_2]_T$, at a 10°C temperature approach on the equivalent work consumed by the process is calculated by this model. The results show that with low rich P_{CO2}, the three solvents have equivalent capacities and the equivalent work for stripping are comparable. However, with richer solutions, the generic solvent A requires less work. A minimum equivalent work of stripping is observed when the rich P_{CO2} ~ 8kPa for all three generic solvents. The multipressure stripper reduces equivalent work by ~ 15%.

Experimental (Model Formulation)

Aspen Custom Modeler® (ACM) Model

A model has been developed in Aspen Custom Modeler® to simulate the stripper operation. The model was designed for a wide variety of solvents but has currently been applied to a 7m MEA and the generic solvents.

Modeling Assumptions

(a) The sections were assumed to be well mixed in the liquid and vapor phases.

(b) The reboiler was assumed to be in equilibrium.

The CO_2 vapor pressure (kPa) under stripper conditions are represented by the linear expression

$$\ln P = a + b*[CO_2]_T + \frac{c}{T} + d\frac{[CO_2]_T^2}{T^2} + e\frac{[CO_2]_T}{T^2} + f\frac{[CO_2]_T}{T} \quad (1)$$

P = the equilibrium partial pressure of CO_2 in kPa

T = temperature in Kelvin

$[CO_2]_T$ = total CO_2 concentration (m)

The adjustable constants (Table 4) were obtained by regressing the points for 7m MEA from equilibrium flashes in Aspen Plus® using the rigorous model developed by Freguia (2002) from data of Jou and Mather (1995). For the generic solvents the constant, b, was changed from –6.43 to –6.6, -5.43 and –4.43. This alters the capacity of the solvent for CO_2 desorption.

Table 4. Adjustable Constants in VLE Expression

	7m MEA	Generic Solvent A	Generic Solvent B	Generic Solvent C
a	35.12	35.12	35.12	35.12
b	-6.43	-6.6	-5.43	-4.43
c	-14281	-14281	-14281	-14281
d	-11148.5	-11148.5	-11148.5	-11148.5
e	-485777	-485777	-485777	-485777
f	4667.14	4667.14	4667.14	4667.14

The heat of absorption/desorption is calculated by differentiating Equation (1) with respect to 1/T. This is given by the following

$$-\frac{\Delta H}{R} = c + 2d\frac{[CO_2]_T^{\,2}}{T} + 2e\frac{[CO_2]_T}{T} + f[CO_2]_T \qquad (2)$$

where ΔH represents the heat of absorption/desorption [=] kcal/gaol CO_2, and
R is the Universal gas constant [=] cal/K-mol

The rich $[CO_2]_T$ at specified rich P_{CO2} (kPa) leaving the absorber at 60°C for MEA and the three generic solvents is shown in Table 5.

Table 5. Rich $[CO_2]_T$ at Absorber Conditions at 60°C

	$[CO_2]_T$ (m)			
Rich P_{CO2}* (kPa)	7m MEA	Generic A	Generic B	Generic C
1.25	2.73	2.91	2.00	1.58
2.5	2.99	3.20	2.17	1.72
5	3.26	3.49	2.36	1.86
10	3.53	3.79	2.55	2.01

The heat of vaporisation of water, partial pressure of water, heat capacities of steam, CO_2, and the solvent (essentially water) were calculated from equation derived from the DIPPR database.

The equilibrium partial pressure of CO_2 and water on each section were calculated from Equation (3):

$$E_{mv} = \frac{P_n - P_{n-1}}{P_n^* - P_{n-1}} \quad (3)$$

where E_{mv} is the Murphree plate efficiency defined in terms of partial pressures,
P_n, P_{n-1} is the partial pressures of the component on sections n and n-1, and
P_n^* is the equilibrium partial pressure of the component leaving section n.

An efficiency of 40% and 100% were assigned to CO_2 and water. The model assumed a 100% efficiency with respect to heat transfer.

The equivalent work is a convenient way to quantify the heat requirement of the process. It constitutes the work lost from the turbine upstream of the power plant since the condensing steam used to run the reboiler is no longer available to generate electric power. Assuming the enthalpy difference between the feed and products is negligible compared to the heat input and cooling water at 313 K is used to remove heat in the condenser, the equivalent work, W_{eq}, consumed by the process is given by

$$W\,(\text{kcal/gmol}\,CO_2) = Q\left[\frac{T_{cond} - T_o}{T_{cond}}\right] + W_{comp} \quad (4)$$

where Q is the reboiler duty in kcal/gmol CO_2,

T_{cond} is the temperature of the condensing steam (temperature of reboiler plus 10K) in the shell of the reboiler, and

T_o is the temperature of the cooling water (313K).

W_{comp} constitutes the adiabatic work of compression of the gas exiting the top of the stripper to 1000 kPa (an arbitrary pressure selected). For this analysis isentropic efficiency of the compressor was assumed to be 75%.

Results and Discussion

Predicted Stripper Performance

The stripper performance for a simple stripper operating at 160 kPa with five compression stages to compress the gas to 1000kPa with interfolding to 313K between the stages downstream of the stripper was simulated using the three generic solvents.

Table 6 shows the reboiler duty, total equivalent work, and optimum capacity for the three generic solvents. The results show that the generic solvent with a slightly lower heat of desorption (Generic A) than 7m MEA has a slightly higher capacity than the other two solvents.

Table 6. Stripper Performance for Three Generic Solvents

				Rich	Lean	Optimum Capacity
	P_{CO2} (kPa)	Q_{reb} (kcal/gmol CO_2)	Total W_{eq} (kcal/gmol CO_2)	$[CO_2]_T$ (m)		
Generic A	1.25	62.97	17.93	2.91	2.27	0.64
	2.5	49.25	14.39	3.20	2.36	0.84
	5	40.61	12.00	3.49	2.45	1.04
	10	34.81	10.56	3.79	2.54	1.25
Generic B	1.25	58.05	16.81	2.00	1.35	0.65
	2.5	49.77	14.63	2.17	1.37	0.80
	5	43.49	13.00	2.36	1.37	0.99
	10	39.13	11.87	2.55	1.37	1.18
Generic C	1.25	59.46	17.24	1.58	0.98	0.60
	2.5	51.78	15.23	1.72	0.98	0.74
	5	46.43	13.84	1.86	0.97	0.89
	10	42.29	12.77	2.01	0.96	1.05

Figure 8 shows the total equivalent work and optimum capacity for the three generic solvents. With a low rich P_{CO2}, the three solvents have equivalent capacities and the equivalent work for stripping is comparable. However, with richer solutions, the generic solvent A requires less work. A minimum equivalent work of stripping is observed when the rich P_{CO2} ~ 8kPa.

Table 7 shows the results obtained with the multipressure system when the rich P_{CO2}* = 5kPa with the stripper operated at 500kPa/280kPa/160kPa pressure levels and subsequently the CO_2 is compressed to 1000kPa. The capacity of generic A increased by 10% while that of Generics B and C decreased by 4% and 9%, respectively. This suggests that a generic solvent that behaves much like 7m MEA but with a lower heat of desorption will have a greater capacity for CO_2.

Conclusions and Future Work

In this quarter, the ACM model was extended to incorporate three generic solvents. A minimum equivalent work of stripping is observed when the rich P_{CO2} ~ 8kPa for all three solvents. The multipressure stripper reduces equivalent work by ~ 15%. In the next quarter, a mass transfer rate model will be developed to predict the height of packing required to perform the stripping of CO2 using various solvents with minimum energy consumption.

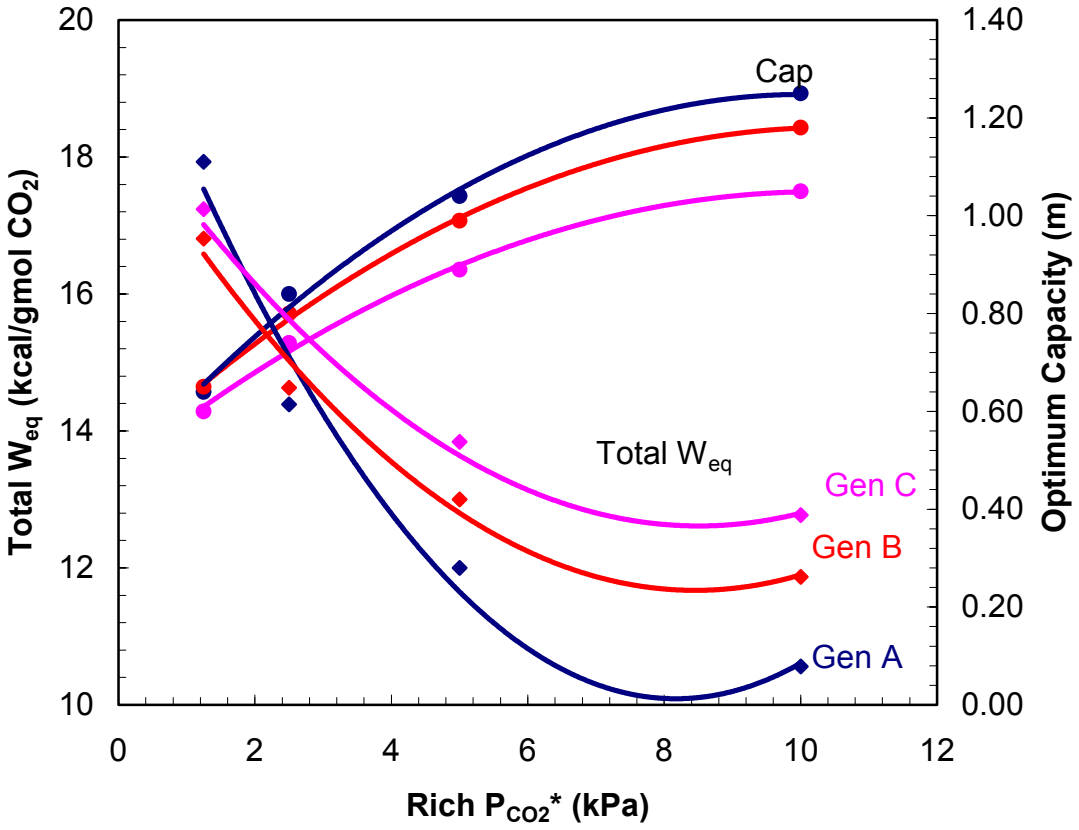

Figure 8. Performance Curves for Generic Solvents

Table 7. Performance of Generic Solvents with Multipressure Stripper, Rich P_{CO2}*= 5kPa

	Q_{reb}	Total W_{eq}	ΔH_{des} in reboiler	Rich	Lean	Optimum Capacity
	(kcal/gmol CO_2)			$[CO_2]_T$ (m)		
Generic A	23.36	10.48	18.5	3.49	2.33	1.16
Generic B	30.33	11.27	21.7	2.36	1.41	0.95
Generic C	34.32	12.07	23.8	1.86	1.04	0.82

Task 2 – Pilot Plant Testing

Subtask 2.5a – Campaign 2 Pilot Plant - Results for Absorber

by Eric Chen
(Supported by EPA Star Fellowship)

Introduction

In this quarter, modifications were made to the pilot plant before the commencement of the second CO_2 capture campaign. The second campaign began in mid-October and was completed in early-November. A total of 21 runs were completed. There were some issues related to CO_2 loading analysis and we are in the process of resolving it.

Experimental

In the first campaign, there were issues of material balance closure across the absorber column. It was believed that the rich samples were flashing. Therefore, sample bombs were constructed and used to take samples. The sample bombs consisted of two 0.5-inch Swagelok quick-connects and 0.5-inch diameter stainless tubing, 7.5 inches in length. The sample bombs had a volume of approximately 10mL. The sample bombs were connected to the sample hoses and liquid was allowed to circulate for several minutes before it was disconnected.

For samples taken off the sample pump, the discharge valve was always shut first and then the suction side valve was closed. The sample bombs were colored coded to match the sample location. Samples were taken from five different points: absorber lean, absorber middle, absorber rich, stripper lean, and stripper middle. The samples were extracted from the sample bomb using a syringe. Approximately 10mL of sample was injected through a septum into a sample vial containing 30mL of chilled DI water. The sample was injected underneath the surface of the DI water. Therefore, the samples were all diluted to minimize any flashing.

The solvent from the first campaign was used in the second campaign. The solvent has been stored in steel drums between the two campaigns. The pilot plant was operated for a total of eight days and approximately 24 hours each day. Twenty-three runs were conducted at approximately a single solvent composition. The piperazine and potassium concentration varied between 1.3 to 1.4 mol/ kg solvent and 2.8 to 2.9 mol/kg solvent, respectively. The gas and liquid flowrates varied from 1.2 to 2.2 kg/m^2-s and 2.7 to 11.9 kg/m^2-s, respectively. The L/G ratio varied from 1.8 to 6.9 kg/kg. The inlet CO_2 concentration varied between 2.6 to 12.4 mole percent and the inlet gas temperature varied between 30 and 50°C. The inlet temperature of the solvent to the absorber was maintained nominally at 40°C. The stripper pressure was varied between 0.3 to 1.8 atm. The absorber contained 20 ft of Flexipac 1Y structured packing and the stripper contained 40 ft of IMTP #40 random packing. The CO_2 penetration varied from 0.03 to 0.4. No additional vanadium was added to the system. Based on preliminary analysis, the lean loading varied from 0.43 to 0.53 mol/total alkalinity. The lean density varied between 1221 to 1230 kg/m^3.

In order to increase the inlet gas temperature, a bypass around the blower was constructed. A six-inch PVC pipe run was added towards the beginning of the second campaign. As a result, water began to condense out downstream of the knock out pot and accumulated in some of the lines, leaking out through the blower casing. Water was periodically drained from the lines and pumped back into the system.

The condensation of water eventually led to the non-operation of the gas inlet Vaisala CO_2 analyzer. Therefore, the Horiba was used to measure the inlet CO_2 gas concentration and no middle gas samples were analyzed. There was some lag time associated with the extractive Horiba gas sampling system and, as result, the system was difficult to control at times and reached steady state over longer time periods.

Both of the online Rosemount pH meters were replaced prior to the commencement of the second campaign. The inlet pH meter was hardwired to the transmitter while the outlet pH meter still had the quick-disconnect cabling. Unfortunately, the outlet online Rosemount pH meter failed just before the commencement of the second campaign. The cause of the failure is still under investigation.

Anti-foam was used throughout the second campaign. A new anti-foam from GE was used in the second campaign, which the manufacturer claimed to be better suited for our solvent system. The inlet loading was monitored by the online Rosemount pH meter and controlled by either the addition of makeup CO_2 or increasing the stream flow to the stripper reboiler. Piperazine and potassium concentrations were determined by titration with hydrochloric acid and sodium hydroxide and were reported as total alkalinity.

Towards the end of the second campaign, it was discovered that the CO_2 calibration gases were not in mole percentage as previously assumed, but in weight percent. The correction was applied to the data from the first campaign and to the runs made during the second campaign. The material balance from the first campaign matched up better than before and was not systematically off by 30%. The updated plot of rate comparison data and VLE are shown in Figures 9 and 10.

Results and Discussion

The results from the absorption of CO_2 into the piperazine/potassium carbonate solvent are shown in Table 8. Approximately ten titrations were performed at the beginning and end of each concentration change, which was when the water was added back into the system. Thus, the piperazine to potassium ratio was calculated as the average of the beginning and end ratios. The piperazine concentration was then back-calculated based on this average ratio.

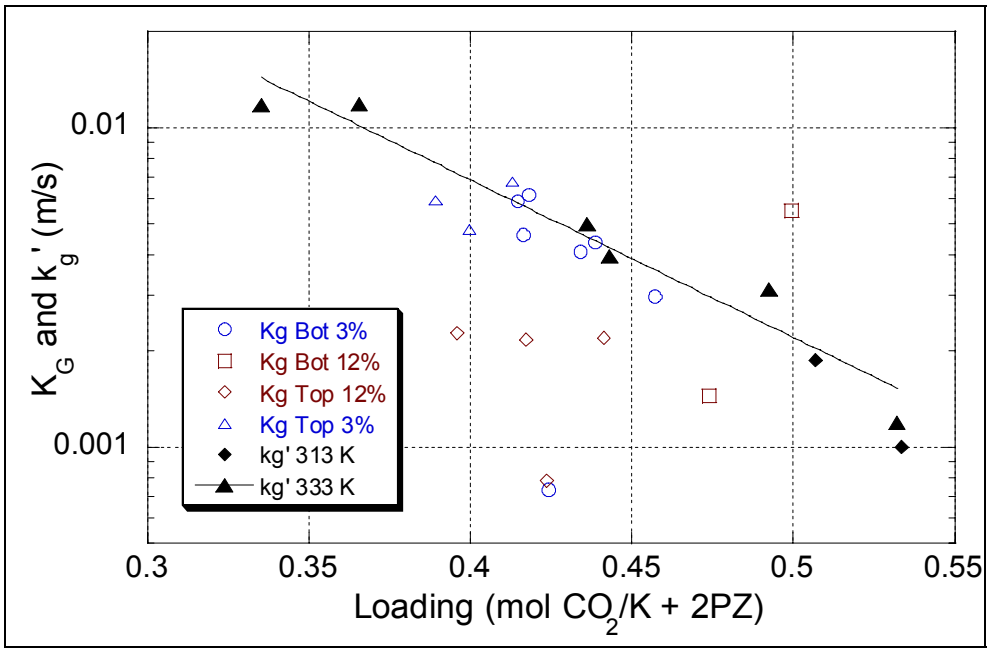

Figure 9. Wetted Wall Column and Campaign 1 Rate Data

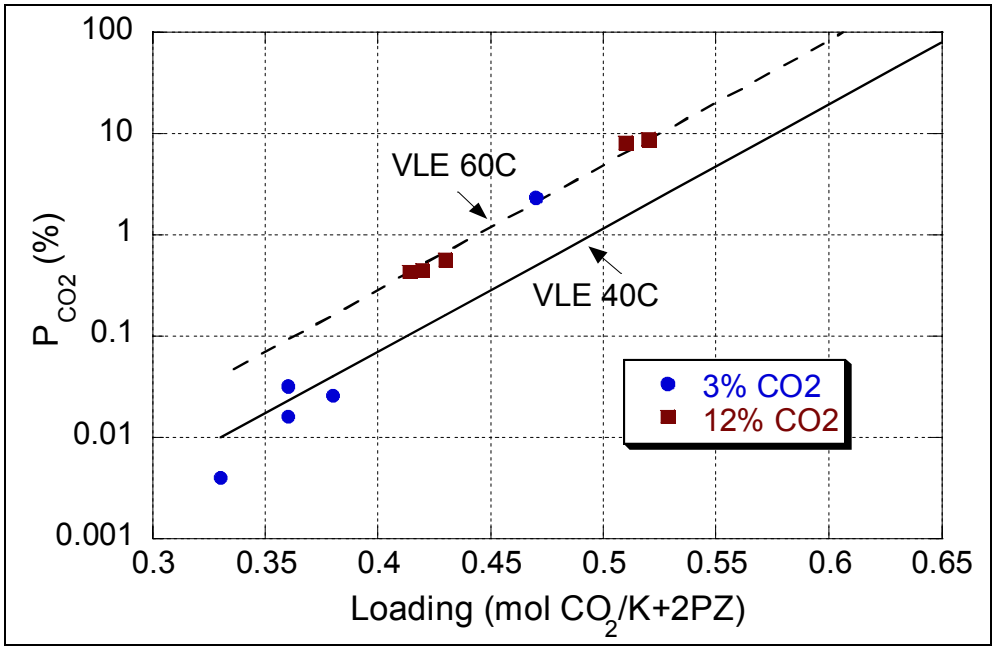

Figure 10. Pinched Data Points from Campaign 1

Table 8. Absorber Results Table

Run #	Date/Time	Ln Total Alkalinity 2PZ+K$^+$	Lean PZ mol/kg solv	Loading mol/Alk[1]	K+/PZ	Capacity		CO2 In %	CO2 Out %	CO2 Penetration[2]	G kg/m2-solv	L kg/m2-solv	L/G kg/kg	Temp Gas In K	Temp Gas Out K	Temp Liq In K	Temp Liq Out K
						Liq mol/kg solv	Gas mol/kg solv										
2.1	10/26/04 10:47	5.38	1.27	0.43	2.24	0.92	1.11	7.59	1.23	0.16	2.16	4.31	2.00	322.38	322.03	313.32	320.55
2.2	10/26/04 14:45	5.42	1.28	0.08	2.24	-0.41	0.90	8.27	3.25	0.39	2.12	4.20	1.99	327.26	323.87	314.29	323.79
2.3	10/27/04 0:15	5.42	1.28	0.48	2.24	0.85	0.63	7.76	2.62	0.34	1.64	4.88	2.97	319.36	318.23	313.90	317.98
2.4	10/27/04 2:30	5.43	1.28	0.48	2.24	0.64	0.61	8.30	2.09	0.25	1.66	5.87	3.54	318.85	314.00	313.74	317.74
2.5	10/27/04 3:30	5.44	1.28	0.04	2.24	0.59	0.54	7.25	1.57	0.22	1.64	6.10	3.71	319.90	313.80	313.75	317.83
2.6	10/27/04 6:00	5.45	1.29	0.49	2.24	0.54	0.51	7.08	1.15	0.16	1.64	6.67	4.06	320.38	311.87	314.42	319.12
2.7	10/27/04 7:00	5.77	1.38	0.51	2.18	0.32	0.53	7.59	1.29	0.17	1.63	6.89	4.23	321.36	312.61	314.41	319.55
2.8	10/27/04 13:00	5.44	1.29	0.50	2.23	0.64	0.61	7.92	2.25	0.28	2.14	7.22	3.38	325.23	319.06	314.54	320.42
2.9	10/28/04 5:15	5.62	1.38	0.47	2.07	0.61	0.57	7.85	2.07	0.26	1.34	4.57	3.42	309.98	315.11	313.90	315.30
2.10	10/28/04 14:55	5.60	1.36	0.47	2.12	0.57	0.51	8.32	1.15	0.14	1.28	6.22	4.87	320.80	311.79	314.36	321.17
2.11	10/28/04 17:15	5.59	1.35	0.47	2.14	0.51	0.48	7.92	1.11	0.14	1.24	6.18	4.97	324.45	312.45	314.55	321.61
2.12	10/28/04 20:15	5.60	1.35	0.50	2.14	0.87	0.51	7.89	0.28	0.03	1.24	6.40	5.18	326.96	310.50	314.15	321.27
2.13	10/29/04 6:45	5.56	1.34	0.50	2.15	0.47	0.55	8.23	1.70	0.21	1.36	5.43	3.98	305.91	311.67	313.61	317.83
2.14	11/2/04 21:45	5.56	1.35	0.52	2.13	0.52	0.48	3.26	0.52	0.16	1.35	2.73	2.02	302.24	311.11	316.48	303.86
2.15	11/3/04 1:30	5.65	1.38	0.48	2.10	0.44	0.46	3.61	0.45	0.12	1.35	3.15	2.33	302.97	309.54	315.11	307.75
2.16	11/3/04 6:15	5.75	1.41	0.48	2.07	0.52	0.50	2.90	0.42	0.15	1.71	3.02	1.77	305.54	308.32	312.00	303.85
2.17	11/3/04 12:30	5.52	1.36	0.52	2.07	0.37	0.29	2.63	0.52	0.20	1.68	4.29	2.55	309.27	312.29	317.94	310.46
2.18	11/3/04 16:45	5.49	1.34	0.53	2.09	0.31	0.26	2.62	0.22	0.08	1.67	5.39	3.23	311.40	314.04	320.34	314.22
2.19	11/4/04 7:30	5.58	1.36	0.46	2.09	0.74	0.57	11.26	1.16	0.10	1.84	11.07	6.02	321.68	309.61	313.28	321.34
2.20	11/4/04 11:15	5.53	1.34	0.50	2.11	0.68	0.55	11.61	0.84	0.07	1.71	11.87	6.92	334.47	310.07	313.61	322.71

Run #	Date/Time	Ln Total Alkalinity 2PZ+K^+	Lean PZ mol/kg solv	Loading mol/Alk[1]	K+/PZ	Capacity		CO2 In %	CO2 Out %	CO2 Penetration[2]	G kg/m2-solv	L kg/m2-solv	L/G kg/kg	Temp Gas In K	Temp Gas Out K	Temp Liq In K	Temp Liq Out K
						Liq mol/kg solv	Gas mol/kg solv										
2.21	11/4/04 15:15	5.47	1.33	0.50	2.10	0.57	0.59	12.42	1.35	0.11	1.85	11.89	6.43	322.50	312.18	314.53	324.27
2.22	11/4/04 23:00	5.61	1.37	0.48	2.09	0.65	0.73	11.68	2.62	0.22	1.91	8.19	4.28	314.61	313.82	312.96	320.76
2.23	11/5/04 4:45	5.65	1.38	0.45	2.09	0.66	0.78	12.01	2.20	0.18	1.91	8.13	4.25	314.80	314.88	312.82	320.71

1. Loading = mol CO_2/Total Alkalinity
2. Penetration = CO_2,Out/CO_2,I

Conclusions and Future Work

The CO_2 loading analysis for Campaign 2 will need to be completed before further data analysis can be done. In addition, ICP analysis will be done to determine iron and vanadium concentrations. The absorber model will be modified to fit the data obtained from the pilot plant experiments. The MEA baseline campaign is scheduled for late February.

Subtask 2.5b – Campaign 2 Pilot Plant - Results for Stripper

by Babatunde Oyenekan
(Supported by this contract)

Summary

In this quarter, the second pilot plant campaign was carried out. The stripper was equipped with two beds of CMR #2 packing with 10 m of packing in each bed. We report the data obtained during the campaign for the 5m K^+/ 2.5m PZ solvent. These include CO_2 concentrations in the rich and lean solutions, temperature profiles in the column, steam flow, and rates when the stripper is operated at different pressures. Analysis of the data involves estimation of pinched regions, estimation of heat losses, and degree/extent of flashing in the cross exchanger. The results show that lean end pinches occurred in the stripper. The amount of heat required to heat the rich solvent to the temperature of the reboiler constituted 38% to 82% of the actual heat used in the stripping operation. The energy efficiency of the stripper ranged from 57% to 94%.

Experimental

Data Collection

The online stripper inlet and outlet CO_2 concentrations were measured with Vaisala GM CO_2 analyzers. The Vaisala probes were ranged from 0 to 1%, 0 to 5% and 0 to 20% CO_2. The online absorber middle concentration was measured using a Horiba PIR-2000 CO_2 analyzer, which had a range of 0 to 5 % CO_2. The Horiba analyzer could be readily switched to sample the inlet, outlet, or middle of the absorber. The Vaisala measurements were confirmed by the Horiba. The CO_2 analyzers were calibrated before the start of the campaign. At higher CO_2 concentrations, the Horiba analyzer was over-ranged and could not read certain absorber middle concentrations.

Liquid samples of the stripper middle and lean solutions were taken to represent the mid-section and lean concentrations, respectively, while the data from the absorber rich was taken and assumed to be representative of the stripper rich solution. The pH were recorded for each off-line sample with a handheld pH meter. Thermocouples were used to obtain the temperatures in six sections in the stripper. The majority of the samples from the various runs have been analyzed. Piperazine and potassium concentrations were determined by titration with hydrochloric acid and sodium hydroxide and the total was reported as total alkalinity. CO_2 loading was determined by a total organic carbon analyzer (TOC) operating in the mode that gives inorganic carbon. Piperazine and potassium concentration was verified by TOC and inductively coupled plasma (ICP) analysis, respectively. Vanadium and total iron were determined by ICP.

Results and Discussion

Stripper Performance

Table 9 shows the stripper data obtained at 160 to 340kPa pressure at varying CO_2 concentrations in the rich and lean streams. The results show that rich solutions in the

Table 9. Campaign 2 Stripper Data

Run #	Column Pressure (kPa)	Reboiler Level (in)	Reboiler Duty (MMBTU/hr)	PrsDrp (low) (inH_20)	PrsDrp (high) (inH_20)	Feed Temp (K)	Top Temp (K)	Bot Temp (K)	Steam Pressure (psia)	Steam Flow (lb/hr)	Steam Temp (K)	% Valve opening
	160	13.43	1.48	5.26	5.03	353.67	384.52	390.52	120.52	1559	444.66	
2.1	155	12.33	1.57	5.59	5.28	353.42	384.10	389.44	120.56	1649	444.26	
2.2	160	14.44	1.75	5.96	6.24	353.28	386.05	390.63	118.82	1843	443.74	
2.3	163	7.86	0.82	1.63	1.42	350.60	379.25	391.10	128.46	851	447.63	13.14
2.4	160	6.52	0.92	2.25	2.00	346.61	375.74	390.65	126.88	954	447.19	13.35
2.5	156	6.94	0.92	2.69	2.42	346.06	374.46	389.68	123.28	952	445.32	13.44
2.6	163	6.63	0.98	3.61	3.39	349.48	376.13	391.29	121.92	1019	445.10	22.00
2.7	165	6.92	0.98	3.34	3.14	349.78	376.65	391.91	121.76	1019	445.14	22.00
	155	5.62	1.09	4.45	4.25	348.74	374.05	389.92	120.89	1134	444.82	22.00
2.8	153	5.55	1.09	5.96	6.01	349.84	373.75	389.23	120.87	1132	444.85	22.00
	181	7.88	0.69	0.36	0.09	350.63	374.65	394.78	129.82	718	448.05	14.00
2.11	171	7.35	0.63	0.35	0.08	350.97	372.62	393.23	128.83	658	447.85	14.00
	155	6.80	1.04	3.65	3.46	348.56	376.39	389.98	121.77	1077	445.27	14.00
	155	6.90	1.04	4.73	4.48	348.98	376.81	389.93	121.35	1075	445.18	14.00
	153	6.95	1.04	4.39	4.03	352.58	377.21	389.42	121.13	1075	444.93	28.00
	159	6.67	1.14	5.35	5.12	351.18	377.31	390.47	121.01	1184	444.99	20.19
	159	6.57	1.26	5.96	6.80	350.89	379.27	390.74	120.44	1316	444.59	20.34
	340	6.18	0.89	0.55	0.27	347.21	345.59	415.29	128.64	968	447.44	12.87
	343	6.11	0.89	0.59	0.30	346.30	341.16	415.77	127.83	969	447.25	12.90

160 to 180kPa cases were subcooled liquids. This is evident by the sharp increase in temperature of the liquid solution as the rich solution enters the stripper. When the stripper is operated at 340 kPa, it is observed that flashing occurs at the stripper inlet. The rich solution temperature decreases slightly at the stripper inlet. The approach temperature in the cross exchanger is observed to be very large ranging from 36K to 70K. This driving force could be even larger as flashing of the rich solution occurred in the cross exchanger. This would have lowered the temperature of the solution as it exits the exchanger and thereby require more energy to raise the temperature of the stripper inlet to the temperature of the reboiler. The location of the steam pressure valve for the cross exchanger will be changed from upstream of the exchanger to downstream of the exchanger in future campaigns in order to get better temperature and reboiler duty measurements. Table 10 delineates the reboiler duty calculated into its constituent parts. It also provides an estimate of the heat loss in the system.

$$\text{Heat loss} = \text{Reboiler duty} - (\text{Sensible heat} + \text{stripping steam} + H_{vap}, H_2O$$

$$\text{Energy efficiency} = \frac{\text{Re boiler duty} - \text{Heat loss}}{\text{Re boiler duty}}$$

Table 10. Energy Efficiency of Stripping Operations

Column P (kPa)	Gas in %	Gas out %	Reboiler Duty (MMBTU/hr)	Sensible heat MMBtu/hr	Stripping steam MMBtu/hr	H_{vap}, H_2O MMBtu/hr	Heat loss MMBtu/hr	Energy Efficiency %
153	0.15	0.05	1.09	0.48	0.18	0.04	0.39	64.57
181	0.09	0.03	0.69	0.46	0.18	0.06	0.38	64.64
171	0.09	0.03	0.63	0.34	0.11	0.07	0.17	74.76
155	0.10	0.02	1.04	0.32	0.11	0.02	0.18	71.93
155	0.09	0.02	1.04	0.43	0.14	0.03	0.44	57.45
153	0.09	0.01	1.04	0.43	0.14	0.08	0.40	61.84
159	0.09	0.00	1.14	0.39	0.13	0.07	0.44	57.49
343	0.10	0.02	0.89	0.61	0.13	0.10	0.06	93.58

The energy efficiency of the stripping operations varied from 62 to 94%. Of the amount of energy that was actually used in the stripping operation, the sensible heat required to raise the temperature of the rich solution to that of the reboiler duty constituted between 38% and 82%. Heavy heat losses were observed and these constituted between 6% and 27% of the total steam input into the column.

In order to have an idea of the internal column operation, temperature profiles in the column were plotted. This would give some insight into phenomena such as the existence of pinches and their location. Figure 11 shows representative temperature

profiles for different parts of the column under vacuum (32kPa), atmospheric (160kPa), and above atmospheric (340kPa) pressure conditions.

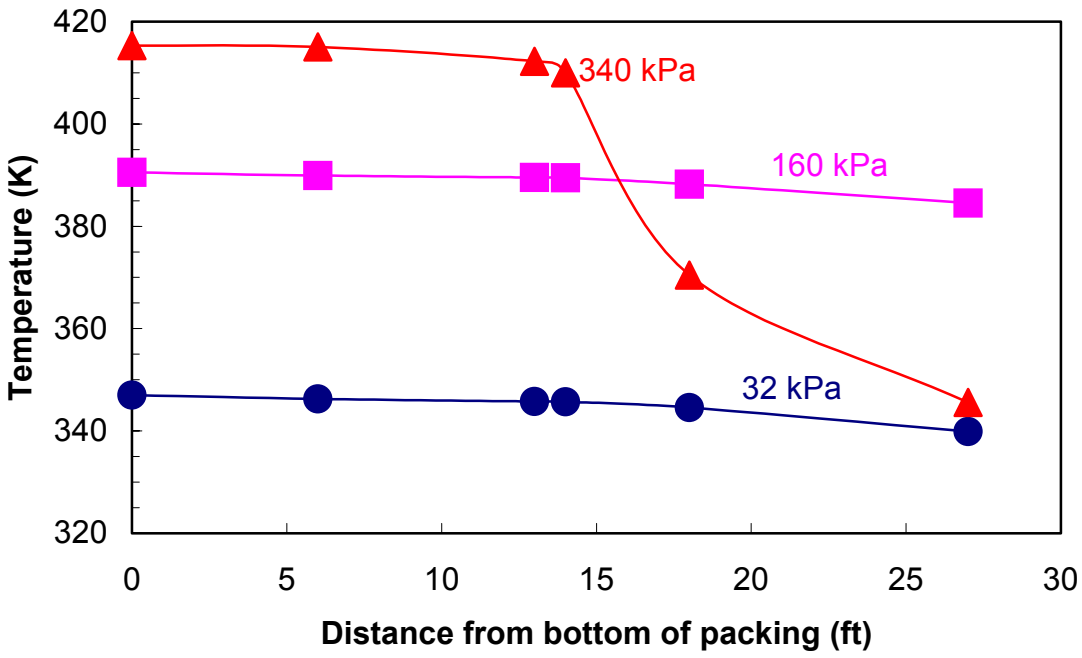

Figure 11. Temperature Profiles in the Stripper at Different Pressures to Yield 85% Removal

The plot shows that the reboiler temperature rises as the pressure in the column rises. The difference in temperature between the top and he bottom section of the column is about 5K for the vacuum and atmospheric pressure columns but varies by up to 70K for the 340 kPa pressure column. For the vacuum and atmospheric columns, there seems to be a lean end pinch but the lean end pinch in the 340kPa column is quite distinct.

The capacity of the solvent was calculated based on data collected that were used for TOC and titration analysis. Table 11 shows the results of the liquid sample analysis. The capacity of the liquid solvent is seen to vary from 0 to 1.47 mol CO_2 / kg solvent. There are some outliers though which could be due to some error in the sampling of the solution.

Table 11. Liquid Phase Analysis for Stripper

Sample Date	Sample ID		Analysis Dilution			TOC Raw	Undiluted		Liq. Cap mol/kg soln
			DI g	DI+S g	Sample g	IC ppm	IC ppm	CO2 Ldg mol/kg	
10/26/2004	AR	1	38.3044	39.0064	0.7020	188.6	36981	3.08	3.08
10/26/2004	SL	1	-	-	-				
10/26/2004	AR	2	38.3829	38.9719	0.5890	47.7	11903	0.99	0.01
10/26/2004	SL	2	38.2147	38.8739	0.6592	52.67	11806	0.98	
10/26/2004	AR	3	38.4176	39.1239	0.7063	99.61	19015	1.58	0.49
10/26/2004	SL	3	38.3072	39.0810	0.7738	74.6	13119	1.09	
10/27/2004	AR	6	41.5078	41.9350	0.4272	15.83	5879	0.49	-0.13
10/27/2004	SL	6	40.5078	40.9902	0.4824	10.2	7380	0.61	
10/27/2004	AR	7	38.1855	38.6627	0.4772	19.51	5784	0.48	-0.18
10/27/2004	SL	7	39.0344	39.5410	0.5066	28.18	7900	0.66	
10/27/2004	AR	8	38.2228	38.7741	0.5513	131.7	31810	2.65	0.49
10/27/2004	SL	8	37.6167	38.1089	0.4922	98.31	25875	2.15	
10/27/2004	AR	9	35.0614	35.5410	0.4796	34.3	9104	0.76	0.37
10/27/2004	SL	9	39.2706	39.8010	0.5304	16.56	4688	0.39	
10/27/2004	AR	10	38.2088	38.7694	0.5606	8.085	2003	0.17	-0.53
10/27/2004	SL	10	37.6698	38.2472	0.5774	32.17	8426	0.70	
10/27/2004	AR	11	38.0107	38.5254	0.5147	34.52	9867	0.82	-0.72

Sample Date	Sample ID	Analysis Dilution			TOC Raw	Undiluted		Liq. Cap mol/kg soln
		DI g	DI+S g	Sample g	IC ppm	IC ppm	CO2 Ldg mol/kg	
10/27/2004	SL 11	38.0013	38.5242	0.5229	62.21	18505	1.54	
10/27/2004	AR 12	37.4771	37.9733	0.4962	65.38	16725	1.39	0.55
10/27/2004	SL 12	38.1186	38.6020	0.4834	37.03	10169	0.85	
10/27/2004	AR 13	38.3154	38.9287	0.6133	124.1	27066	2.25	1.47
10/27/2004	SL 13	38.3283	38.8543	0.5260	36.79	9421	0.78	
10/28/2004	AR 14	38.2834	38.8732	0.5898	130.2	33504	2.79	1.04
10/28/2004	SL 14	38.3908	38.9777	0.5869	83.34	20960	1.75	
10/28/2004	AR 15	40.0924	40.6414	0.5490	128.8	33473	2.79	0.59
10/28/2004	SL 15	38.3222	38.9085	0.5863	107.6	26413	2.20	
10/28/2004	AR 16	38.4900	38.9776	0.4876	124.6	33626	2.80	0.66
10/28/2004	SL 16	38.6263	39.1143	0.4880	94.62	25651	2.14	
10/28/2004	AR 17	38.4236	39.0406	0.6170	87.82	18646	1.55	-0.68
10/28/2004	SL 17	38.4271	38.9459	0.5188	104.7	26850	2.24	
10/28/2004	AR 18	38.4103	38.9034	0.4931	115	32200	2.68	0.31
10/28/2004	SL 18	39.7286	40.1846	0.4560	94.09	28532	2.38	
10/28/2004	AR 19	38.6589	39.2609	0.6020	133.6	31295	2.61	0.43

Conclusions and Future Work

In this quarter, the second pilot plant campaign was run. The stripper was equipped with CMR# 2 packing and the solvent used was 5m K^+/ 2.5m PZ solvent. Data for vacuum, atmospheric, and above atmospheric pressure conditions in the stripper were obtained. The results show that lean end pinches occurred in the stripper. Larger temperature variations within the column were observed for the higher than atmospheric stripper while a temperature change of only 5K was observed for the atmospheric and vacuum operations. The amount of heat required to heat the rich solvent to the temperature of the reboiler constituted 38% to 82% of the actual heat used in the stripping operation. The energy efficiency of the stripper ranged from 62% to 93%. Mass transfer rate modeling of this work is ongoing and should be presented in the next report.

Subtask 2.7a – MEA Baseline Campaign – Development of Online Conductivity Measurements

by Ross Dugas
(Supported by this contract)

Introduction

This report presents the relationships observed among monoethanolamine (MEA) concentration, temperature, ionic conductivity, and CO_2 loading of MEA solutions. The goal of this project is to create a real-time indication of CO_2 loading by measurement of the other parameters. This real-time loading will be very useful in reaching and maintaining operating conditions in the pilot plant.

The experiments and analysis of data were performed by Rachel Beveridge, Dan-Tam Nguyen, and Sue Oslund. The group was part of a Special Projects course taught by Dr. Gary Rochelle and supervised by Ross Dugas.

Experimental

Samples of 45, 30, 25, and 15 wt% MEA solutions were prepared from a pure MEA stock and distilled water. At each of these MEA concentrations, samples were prepared which had CO_2 loadings of 0.5, 0.4, 0.2, and 0.0 moles CO_2/mole MEA. These solutions were created by mixing unloaded MEA solutions with CO_2-sparged MEA solutions of the same MEA concentration.

The 16 solutions were analyzed by a Mettler Paar DMA46 densitometer at a temperature of 35.5°C, the maximum allowed by the equipment. The solutions were also analyzed by a Mettler Toledo InLab 730 conductivity sensor at a temperatures ranging from 25 to 60°C. Immediately afterwards, the solution's loading was determined by using an inorganic carbon analyzer. The solutions were injected into the inorganic carbon analyzer three times and the average reading was taken. The conductivity meter used a temperature correction of 2% per °C relative to 25°C and a cell constant of 0.563 cm^{-1}.

Results and Discussion

The raw data collected from the experiments can be seen in Table 12. The adjusted ionic conductivity measurements in Table 12 remove the automatic temperature compensation of 2% per C to give the actual observed ionic conductivity. All of the results from this point forward will be with respect to this non-temperature compensated (absolute) ionic conductivity.

Table 12. Ionic Conductivity, Temperature, and Loading Raw Data

Ionic Conductivity of MEA with CO_2 Loadings

45 wt% MEA		50% Loading		40% Loading				20% Loading				0% Loading		
I.C. (mS/cm)	Adjusted I.C.	Temp(C)	CO2 load (mol/mol)	I.C. (mS/cm)	Adjusted I.C.	Temp(C)	CO2 load (mol/mol)	I.C. (mS/cm)	Adjusted I.C.	Temp(C)	CO2 load (mol/mol)	I.C. (mS/cm)	Adjusted I.C.	Temp(C)
15.38	14.61	22.4	0.52	14.61	13.88	22.4	0.40	10.39	9.85	22.3	0.20			
17.63	19.66	30.5	0.57	16.93	18.73	30.1	0.41	11.3	12.50	30.1	0.22			
23.3	35.88	46.8	0.60	21.4	33.81	48.1	0.42	13.94	21.34	46.5	0.21			
25.5	49.11	58.1	0.52	23.3	45.23	58.5	0.40	15.42	28.94	56.8	0.21			
30 wt% MEA		**50% Loading**		**40% Loading**				**20% Loading**				**0% Loading**		
I.C. (mS/cm)	Adjusted I.C.	Temp(C)	CO2 load (mol/mol)	I.C. (mS/cm)	Adjusted I.C.	Temp(C)	CO2 load (mol/mol)	I.C. (mS/cm)	Adjusted I.C.	Temp(C)	CO2 load (mol/mol)	I.C. (mS/cm)	Adjusted I.C.	Temp(C)
28.4	27.30	23.0	0.41	23.5	23.59	25.2	0.37	13.55	12.87	22.4	0.21	0.549	0.54	24
28.3	31.25	30.0	0.42	24.5	28.31	32.3	0.35	14.75	17.49	33.6	0.21	0.63	0.72	31.4
31	42.56	41.0	0.48	27	38.95	43.5	0.29	16.09	23.39	43.9	0.20	0.671	0.95	42.5
34.2	65.35	57.7	0.38	31.1	61.10	59.1	0.33	18.10	37.81	62.2	0.16	0.726	1.42	58.9
25 wt% MEA		**50% Loading**		**40% Loading**				**20% Loading**				**0% Loading**		
I.C. (mS/cm)	Adjusted I.C.	Temp(C)	CO2 load (mol/mol)	I.C. (mS/cm)	Adjusted I.C.	Temp(C)	CO2 load (mol/mol)	I.C. (mS/cm)	Adjusted I.C.	Temp(C)	CO2 load (mol/mol)	I.C. (mS/cm)	Adjusted I.C.	Temp(C)
29.1	28.98	24.8	0.38	23.9	23.81	24.8	0.30	14.14	14.00	24.5	0.22	0.716	0.71	24.4
30.7	36.69	34.0	0.45	25.5	29.88	33	0.39	14.93	17.32	32.5	0.19	0.77	0.91	33.6
32.3	46.22	43.1	0.42	27.3	38.91	42.9	0.37	16.01	22.51	42.2	0.17	0.806	1.17	43.8
35.6	74.22	62.1	0.38	30.2	59.68	59.4	0.35	17.55	33.74	58	0.18	0.842	1.72	61
15 wt% MEA		**50% Loading**		**40% Loading**				**20% Loading**				**0% Loading**		
I.C. (mS/cm)	Adjusted I.C.	Temp(C)	CO2 load (mol/mol)	I.C. (mS/cm)	Adjusted I.C.	Temp(C)	CO2 load (mol/mol)	I.C. (mS/cm)	Adjusted I.C.	Temp(C)	CO2 load (mol/mol)	I.C. (mS/cm)	Adjusted I.C.	Temp(C)
26	24.40	21.8	0.41	21.3	19.76	21.2	0.35	12.08	11.25	21.4	0.17	0.845	0.79	21.5
28.2	31.07	29.9	0.49	23.3	25.47	29.5	0.38	12.81	14.17	30.1	0.17	0.893	1.01	31.1
29.2	38.68	39.2	0.50	24.1	32.50	40.1	0.38	13.56	17.82	38.8	0.17	0.922	1.21	38.6
31.7	66.09	62.1	0.56	26.1	54.20	61.9	0.40	14.55	28.08	58.2	0.15	0.969	1.96	60.6

*Adjusted IC measurement removes the 2% per °C Temperature Compensation

The ionic conductivity is a strong function of the CO_2 loading in the solution. Elevated temperatures raise the conductivity even further, with larger increases at higher temperatures. These phenomena can be seen below in Figure 12.

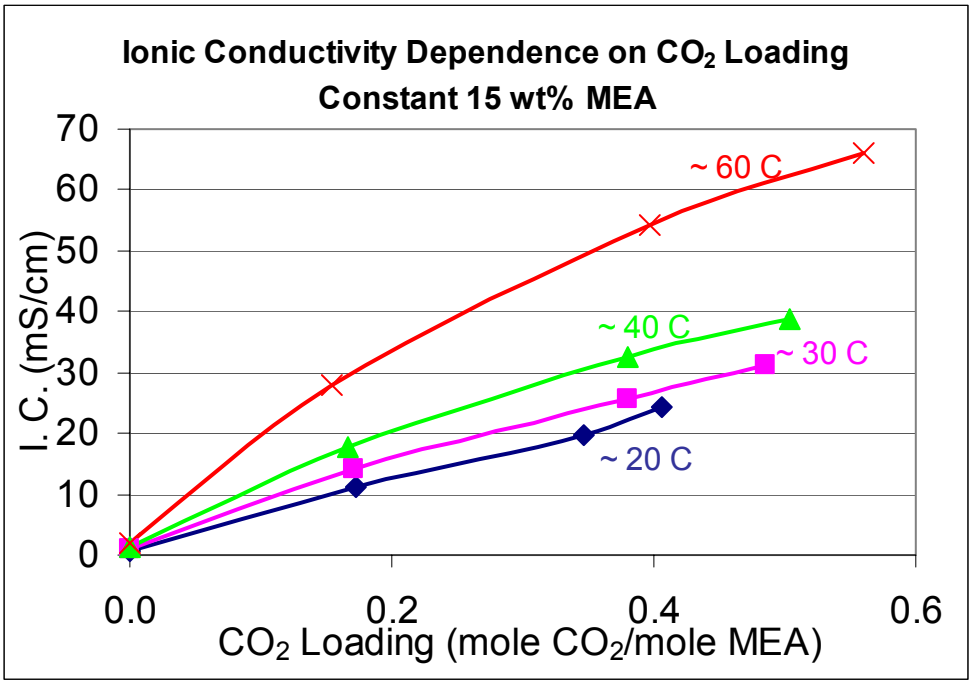

Figure 12. Ionic Conductivity Sensitivity to Loading at 15 Wt% MEA

Although increased MEA concentrations yield more ions for electrical conductance, the increased viscosity of the fluid can effectively decrease the ionic conductivity of the solution. From the experiments performed, the maximum conductivity occurs at approximately 30 wt% MEA. This effect can be seen below in Figure 13.

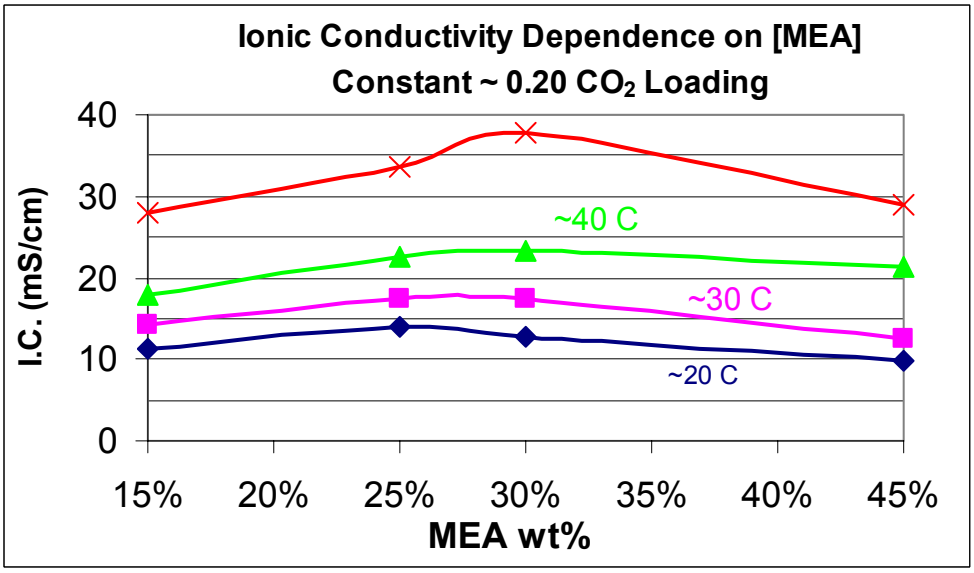

Figure 13. Ionic Conductivity Sensitivity to MEA Wt% at ~0.20 Loading

The goal of this project was to predict CO_2 loading from temperature, ionic conductivity, concentration, and density. Since the conductivity and the density are both dependent variables of the solutions, the density was neglected for the data regression. Three equations were constructed to predict the resultant ionic conductivity. Equation (5) gives a linear model. Equations 6 and 7 give rigorous models, named Rigorous I and Rigorous II, respectively.

$$I.C. = A*(MEAwt) + B*(Temp) + C*[CO_2] + D \tag{5}$$

$$I.C. = A*\ln(MEAwt) + \frac{B}{Temp} + C*\ln([CO_2]) + D \tag{6}$$

$$\ln(I.C.) = A*\ln(MEAwt) + \frac{B}{Temp} + C*\ln([CO_2]) + D \tag{7}$$

From these equations the data was regressed and the predicted ionic conductivity was compared to the observed ionic conductivity. The regressed constants as well of the accuracy of the regressions can be seen below in Table 13.

Table 13. Regressed Parameters and Error Analysis

Results of the Correlation						
Method	Variables				Sum of the Square of the Error	Avg. Percent Error
	A	B	C	D		
Linear	-3.010	0.023	7.826	-5.520	18.945	56.19%
Rigorous I	-19.585	-	13.443	192.468	2.139	21.11%
Rigorous II	-1.089	-2591.145	0.750	9.806	0.201	6.48%

From the error analysis in Table 13, the Rigorous II model was the most accurate. Mathematical rearrangement of the Rigorous II equation yields an equation that will predict the loading of solutions in the pilot plant. This equation can be seen below as Equation (8). This predicted loading will serve as the primary control parameter for pilot plant operations.

$$[CO_2] = \left(\frac{I.C.}{MEAwt^{A}} * \exp - \left(\frac{B}{Temp} + D \right) \right)^{1/C} \tag{8}$$

This real-time loading will be very useful in reaching and maintaining operating conditions in the pilot plant.

References

Aseyev, G. G., and I. D. Zaytsev [translated from Russian by Yu. A. Gorshkov.], *Volumetric Properties of Electrolyte Solutions: Estimation Methods and Experimental Data*, New York. Begell House (1996).

Aseyev, G. G., *Electrolytes: Equilibria in Solutions and Phase Equilibria. Calculation of Multicomponent Systems and Experimental Data on the Activities of Water, Vapor Pressures, and Osmotic Coefficients*, New York: Begell House (1999).

Austgen, D. M., "A Model of Vapor-Liquid Equilibria for Acid Gas-Alkanolamine-Water Systems," Ph.D. Dissertation, The University of Texas at Austin (1989).

Bishnoi, S. and G. T. Rochelle, "Absorption of Carbon Dioxide into Aqueous Piperazine: Reaction Kinetics, Mass Transfer, and Solubility," *Chem. Eng. Sci.* **55**(22): 5531-5543 (2000).

Bishnoi, S. "Carbon Dioxide Absorption and Solution Equilibrium in Piperazine Activated Methyldiethanolamine," Ph.D. Dissertation, The University of Texas at Austin (2000).

Bishnoi, S., and G. T. Rochelle, "Absorption of Carbon Dioxide in Aqueous Piperazine/Methyldiethanolamine," *AIChE J.* **48**(12): 2788-2799 (2002).

Bronsted, J. N., "Acid and Basic Catalysis" *Chem. Rev.* **5**(3): 231-338 (1928).

Cullinane, J. T. and G. T. Rochelle, "Carbon Dioxide Absorption with Aqueous Potassium Carbonate Promoted by Piperazine," *Chem. Eng. Sci.* **59**: 3619-3630 (2004).

Cullinane, J. T., and G. T. Rochelle, "Thermodynamics of Aqueous Potassium Carbonate, Piperazine, and CO_2 Mixtures," *Fluid Phase Equilibria* **227**(2): 197-213 (2005).

Dang, H., "CO_2 Absorption Rate and Solubility in Monoethanolamine/Piperazine/Water," M.S. Thesis, The University of Texas at Austin (2001).

Ermatchkov, V., A. P.-S. Kamps, and G. Maurer, "Chemical Equilibrium Constants for the Formation of Carbamates in (CO2+Piperazine+Water) from 1H-NMR Spectroscopy," *J. Chem. Thermodyn.* **35**(8): 1277-1289 (2003).

Freguia, S., "Modeling of CO_2 Removal from Flue Gases with Monoethanolamine," M.S. Thesis, The University of Texas at Austin (2002).

Hilliard, M., "Thermodynamics of Aqueous Piperazine/Potassium Carbonate/Carbon Dioxide Characterized by the Electrolyte NRTL Model within Aspen Plus®," M.S. Thesis, Department of Chemical Engineering, The University of Texas at Austin (2005).

Jou, F. Y., and Mather A. E. "The Solubility of CO_2 in a 30 Mass Percent Monoethanolamine Solution," *Can. J. Chem. Eng.*, **73**(1): 140-7 (1995).

Oyenekan, B. A,. and G. T. Rochelle, "Stripper Models for CO_2 Capture by Aqueous Solvents," Poster Presentation at GHGT-7, Vancouver, Canada (2004).

Pérez-Salado Kamps, Á., J. Xia, and G. Maurer, "Solubility of CO_2 in (H_2O + Piperazine) and in (H_2O + MDEA + Piperazine)," *AIChE J.* **49**(10): 2662-2670 (2003).

Posey, M. L. "Thermodynamic Model for Acid Gas Loaded Aqueous Alkanolamine Solutions," Ph.D. Dissertation, The University of Texas at Austin (1996).

Tosh, J. S., J. H. Field, H. E. Benson, and W. P. Haynes, "Equilibrium Study of the System Potassium Carbonate, Potassium Bicarbonate, Carbon Dioxide, and Water," U.S. Bur. Mines, Rept. Invest. No. 5484: 23 pp (1959.).